Int. J. Advanced Design and Manufacturing Technology, 2024, Vol. 17, No. 1, pp. 7-21

DOI: 10.30486/ADMT.1403.873792 ISSN: 2252-0406 https://sanad.iau.ir/journal/admt

A Quasi-Analytical Method Algorithm Development in Redesigning the Geometry and Structural Analysis of An Aircraft Propeller and Comparing with the Finite Element Method

Behrooz Shahriari *, Hassan Izanlo
Faculty of Mechanics, Malek Ashtar University of Technology, Iran
E-mail: shahriari@mut-es.ac.ir, Hassanizanlo1998@gmail.com
*Corresponding author

Nedasadat Seddighi
Mechatronic Sanaat Sepahan Co., Isfahan, Iran
E-mail: nsseddighi@gmail.com

Received: 12 October 2023, Revised: 26 November 2023, Accepted: 20 December 2023

Abstract: The aircraft propeller is effective in the performance of the aircraft propulsion system and must have acceptable structural strength. The complex aerodynamic geometry of the propeller makes its analysis more difficult. In this study, dynamic and aerodynamic stresses are calculated using the Finite Element Method (FEM). A structural analysis algorithm based on the quasi-analytical method is developed to evaluate the finite element analysis. In this regard, first, an algorithm is developed to redesign the propeller which performs in a way that by checking the dimensions, the geometry of the quasi-propeller is determined with the same mass and the coordinates of the center of mass. Then, different algorithms are developed to calculate the distribution of mass, moment of inertia, and the cross-section of the quasi-blade geometry. The calculation algorithms of rotational dynamic and aerodynamic stress distribution are developed. The results show that the FEM and the quasi-analytical method are well matched. In this study, the force equivalent to the thrust and the opposite force to the propeller rotation are placed instead of the aerodynamic pressure distribution. The comparison of the results obtained from the quasi-analytical method and the FEM indicates that the overall maximum stress of the system occurs at the root of the propeller and the maximum net stress due to aerodynamic forces occurs in the middle of the propeller geometry. According to the results, the rotational dynamic stress is much higher than the aerodynamic stress. It is also shown that the aerodynamic stress reduces the overall stress of the system.

Keywords: Aircraft Propeller, FEM Method, Stress Analysis, Structural Analysis Algorithm

Biographical notes: Behrooz Shahriari received his BSc in Mechanical Engineering and MSc and PhD degrees in Aerospace Engineering from Malek Ashtar University of Technology in 2002, 2012, and 2016, respectively. His current research interests are structural optimization and artificial intelligence. **Hassan Izanlo** received his MSc in Mechanical Engineering from Sharif University of Technology in 2023. His current research interests are artificial intelligence, optimization, robotic nonlinear dynamics, and nonlinear vibration. **Nedasadat Seddighi** received her MSc in Aerospace Engineering from Malek Ashtar University of Technology. Her field of research is optimization and artificial intelligence.

Research paper

1 INTRODUCTION

Aircraft propeller, as a main part of the propulsion system, plays an important role in the performance of the aircraft. Today, with the advancement of aerodynamic, structure, and manufacturing technology sciences, aircraft designers are looking for propellers with high aerodynamic, propulsion, and structural efficiency, low weight and noise levels, and higher life and reliability. The airplane propeller is under aerodynamic and rotational dynamic loads. The structural study of this part of the airplane is of particular sensitivity and importance. The stress analysis of this part plays an important role in the overall design and reliability of the aircraft. In this regard, using an efficient method and accurate analysis is an important challenge.

In a study, Yeh et al. [1] studied different stresses on the wind turbine blade. They used ANSYS software to analyse the blade stress. One of the deficiencies of their study is the large size of the mesh in the finite element analysis ("Fig.1-a"). According to the figure, a smaller mesh size should be adopted at the blade root. Based on experience, with the reduction of the mesh size, the stress undergoes many changes. In their study, the effect of blade weight is considered.

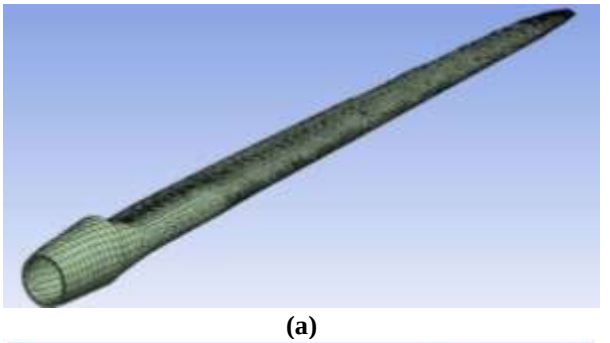

(a)

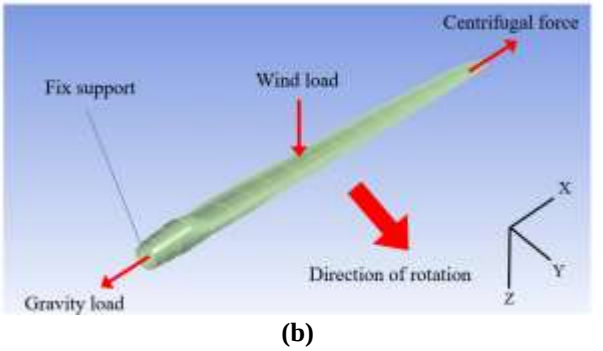

(b)

Fig. 1 Airplane propeller: (a): system meshing, (b): different forces in stress analysis.

The size of the wind turbine blades is large and they have a significant weight, and the stress caused by the weight is also important ("Fig. 1-b"), whereas the weight of the airplane propeller is much less and the stress caused by the weight is negligible. In wind turbines, the length of the blade and the surface area are such that the mass of the blade is very large and the stress caused by the weight becomes one of its important parameters. In their study, the maximum stress was 108 MPa. In many rotating equipment that deal with fluids, the maximum stress is at the blade root. In a study, Srivastava et al. [2] showed that for different vane states, the maximum stress is created at the root of the pump vane, and the stresses caused by the fluid pressure on the vanes usually have a small value. Wind turbines usually have the highest stress caused by fluid pressure among similar equipment. Because they have a long length and as a result, significant bending moments are created in the system. Also, due to having a significant surface area, very large aerodynamic forces are created. In another study, Wu and Yang [3] studied the stresses created in a wind turbine blade. They showed that the stress caused by fluid pressure is equal to 57 MPa. Of course, in their model, this stress is created at a point with a high-stress concentration. This point is located at the root of the blade and many bending moments are created at this point. The amount of this stress is less in the airplane propeller because it has a shorter torque arm length. In another research, Doan et al. [4] obtained the stresses of a wind turbine blade by numerical method. They showed that the maximum stresses are near the blade root. Their finite element model had a large mesh size. They considered centrifugal forces, weight force, and aerodynamic forces. In another similar study, Yeh et al. [5] obtained the stress distribution in a 5 MW wind turbine blade. Also, in a study, Heo et al. [6] studied the structural stresses on a morphing wing airfoils with different internal structures such as honeycomb. They showed that there are stresses of about 270 MPa in the structure, which is significant. Di et al. [7] developed an algorithm for Aeroelastic analysis of horizontal wind turbines. The wind turbines do not have high speed.

In the mentioned studies, there is no suitable method for checking the accuracy of the results. Also, in many of them, there are some problems such as the large size of the element used in the analysis. This issue plays an important role in the final accuracy of the analysis. Also, a precise mathematical model is not used in these studies. The present study deals with the structural analysis of the propeller under rotational dynamic and aerodynamic loads. In this direction, a comprehensive algorithm for redesigning the quasi-propeller geometry and its structural analysis is developed.

2 INTRODUCING THE 3D MODEL MATHEMATICAL MODEL

The three-dimensional model of the propeller has two main parts including the blade and hub and some side parts. Figure 2 shows the 3D model of the propeller. The

material of the propeller blade and hub is 2014-T6 aluminium which is presented in "Table 1". The mass of the rest of the parts which are located inside the hub is insignificant and 1.3 kg in total, and also applied as a point mass and the corresponding moment of inertia. The blade mechanical properties are presented in "Table 2". The flowchart of FEM analysis is presented in "Fig. 3".

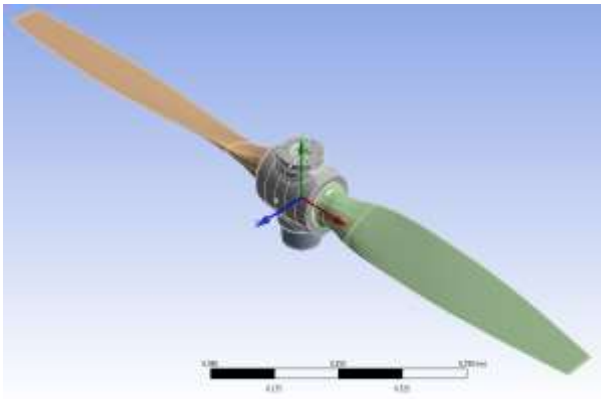

Fig. 2 3D model of airplane propeller.

Table 1 Properties of 2014-T6 aluminum [8]

Properties	Value
density	$2700\,Kg/m^3$
Elastic modulus	$70\,GPa$
Poisson's coefficient	0.33
yielding strength	414 MPa
ε_{P-Y}	0
σ_u	514 MPa
ε_{P-u}	2.08

Table 2 The mechanical properties of the blade

Properties	Value
Total mass	8.08 kg
Center of mass according to Fig. 2	
X	337.5 mm
Y	31.5 mm
Z	7.15 mm

Numerical modeling of rolling bearings and other propeller components is a difficult task. In many studies, fixed constraints are considered, but this issue makes the model far from reality. In this regard, the mathematical model of the propeller is extracted and analysed. Figure 4 shows the mathematical model of the propeller from two views. In the mathematical model, instead of mechanisms and bearings, equivalent springs are used. The symmetry of springing is respected to create mathematical stability. This work is done in such a way that two springs are applied between two surfaces instead of one spring.

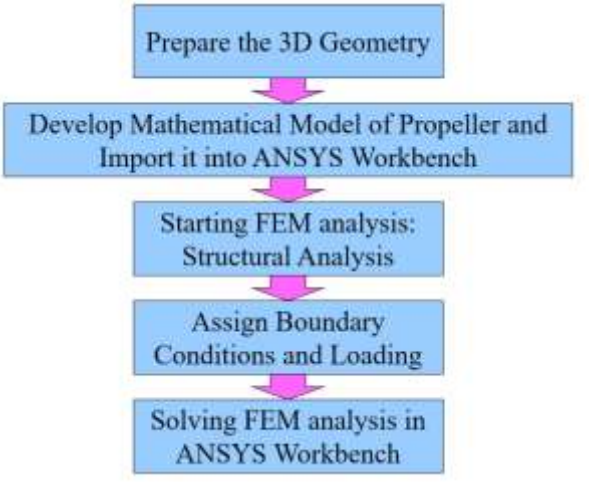

Fig. 3 Structural Analysis of the blade using FEM.

The stiffness of these two springs is half of the original spring. This process creates the closest model to reality. The equivalent stiffness of rolling element bearing is about 10^8 [9]. According to this model, the two surfaces of the blade and the hub can have relative movement. In the case of fixed constraint, relative motion is not applied. This work causes a sharp increase in the natural frequencies of the system and ultimately reduces the accuracy of the solution. The equivalent mass of the rolling bearing is also included in the mathematical model.

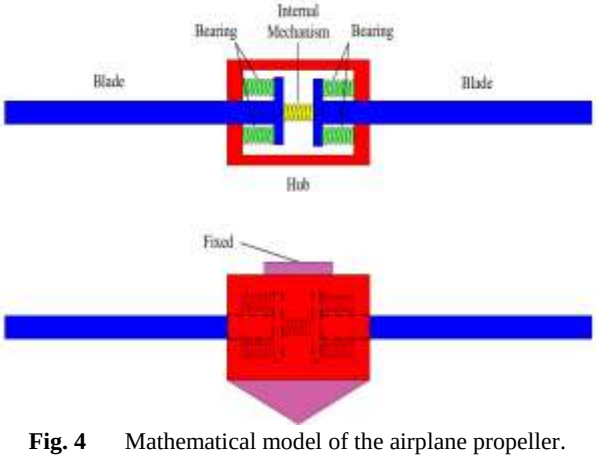

Fig. 4 Mathematical model of the airplane propeller.

3 FINITE ELEMENT MODELING

Due to the complex geometry of the blade and hub, a tetrahedral element with 4 nodes and 12 degrees of freedom is applied to the system. The complex geometry

should be segmented by partition. The blade cannot be partitioned and the hexahedral element cannot be used. The blade geometry is complex due to variable airfoil cross section and also the geometry is twisted. The blade presented in "Fig. 1" does not have any twisting. This element is the best element for sweeping complex geometries such as blades ("Fig. 5"). The elements with more nodes are used for engineering problems with large deformation. The blade structure does not have large deformation during its operation. Therefore, the tetrahedral with 4 nodes is acceptable.

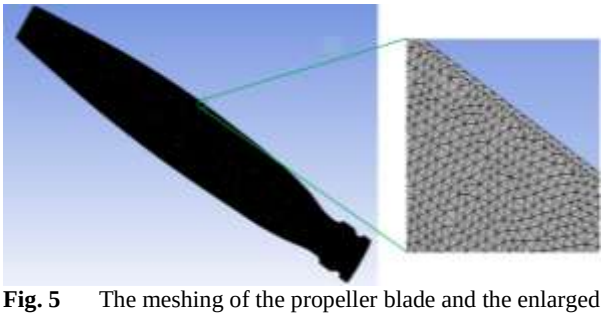

Fig. 5 The meshing of the propeller blade and the enlarged view of its edge.

Figure 6 shows the fully meshed propeller model. The element size in the full model of the airplane propeller is 1.026 mm. The mesh dependency study is continued till the computer system capacity and the final size are selected based on this subject. The complete specifications are shown in "Table 3".

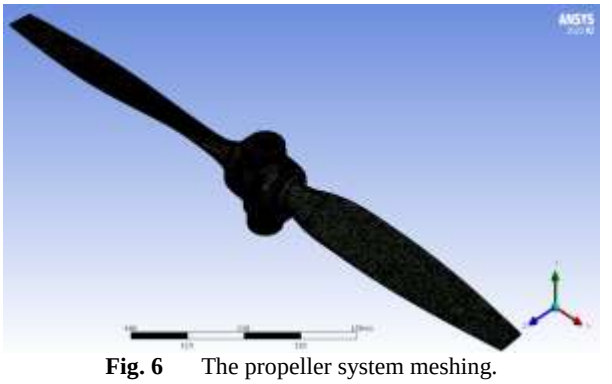

Fig. 6 The propeller system meshing.

Table 3 The final specifications of the aircraft propeller meshing

Mesh specifications	
Mesh type	Tetrahedron
Mesh size	1.026 mm
Number of degrees of freedom of element	4
Mesh characteristic	linear
Total number of elements	2755528
Total number of nodes	4718270

4 STRESS ANALYSIS USING THE FINITE ELEMENT METHOD

The stress analysis of the propeller blade is performed based on the input information provided in "Table 4", which is obtained according to the aerodynamic analysis and the propeller user manual.

Table 4 Input information for structural analysis

Characteristic	**Value**
Maximum working rotational speed	2700 RPM
Maximum propulsion force (related to the maximum working rotational speed)	2073 N
Maximum pressure on the blade	200 KPa
Minimum pressure on the blade	100 KPa

The above information is entered into the finite element analysis. For example, the propulsive force is divided into two equal forces and applied to the propeller in the direction of the airplane's movement, and the opposing forces of the propeller rotation are applied to the system as shown in "Fig. 7", so that they are the closest to reality. To increase the reliability factor of the analysis, the forces entering the system are applied slightly more than the reported forces. Analyzing the aerodynamic force in the case of pressure distribution will be much longer. Figure 7 shows the loading and boundary conditions of the analysis. The ANSYS Workbench distributes load vectors across one or more topologies automatically. This option improves the reality of the problem-solving because the aerodynamics loading is distributed. The loading area (red zone) is shown in "Fig. 7" and the force is not concentrated.

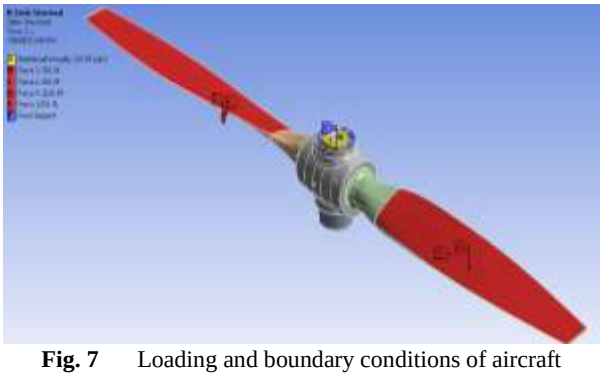

Fig. 7 Loading and boundary conditions of aircraft propeller analysis

Applying the rotational speed to solve will be in the form of D'Alembert. In this case, the dynamic problem is transformed into a static one, and its numerical solution will be much easier. The important point is that the propeller has different tensions at different rotational speeds and different working conditions.

The results of structural stress analysis including rotational dynamic and aerodynamic loads using the finite element method are shown in "Fig. 8". According

to the figure, the maximum stress is at the blade root. The stress in the middle part of the blade also has a large value and the stress gradient between these two points is almost such that it reaches from one high value to another high value. Therefore, in terms of structure, the middle part of the blade is also of special importance. The tension in the root of the propeller is very high due to the presence of a small groove and the consequent increase in stress concentration. Also, drilling continues up to this part and reduces the resistant cross-sectional area.

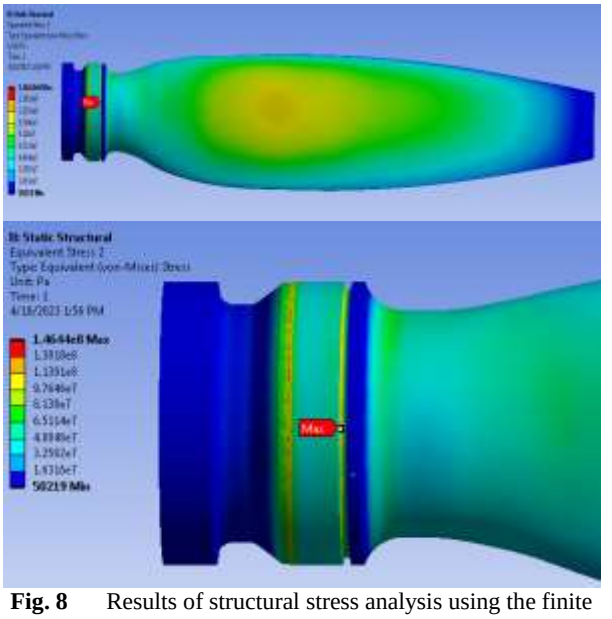

Fig. 8 Results of structural stress analysis using the finite element method.

To investigate the effect of rotational dynamic stress and aerodynamic stress, the finite element analysis of each is done separately. Figure 9 shows the rotational dynamic stresses and "Fig. 10" shows the aerodynamic stresses. According to the stress contour in "Fig. 9", the maximum stress of the structure under the rotational dynamic load is at the root of the blade and its value is slightly higher than the cumulative stress of the dynamic and aerodynamic loads. According to "Fig. 10", the maximum aerodynamic stress is in the middle of the blade. At this point, the blade thickness is low. In bending stress, in addition to the applied bending moment, the equivalent moment of inertia is also important. In the center of the blade, the equivalent moment of inertia is much less than the root of the propeller. The reason for the greater aerodynamic bending stress in the center compared to the root is the same issue. The eccentricity of each cross-section also decreases with the distance from the center of the blade, which reduces the bending moment. This problem will also affect the bending stress created. According to the results of stress analysis, aerodynamic stress is opposed to rotational dynamic stress.

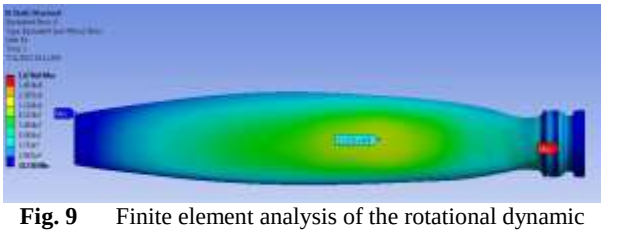

Fig. 9 Finite element analysis of the rotational dynamic stresses.

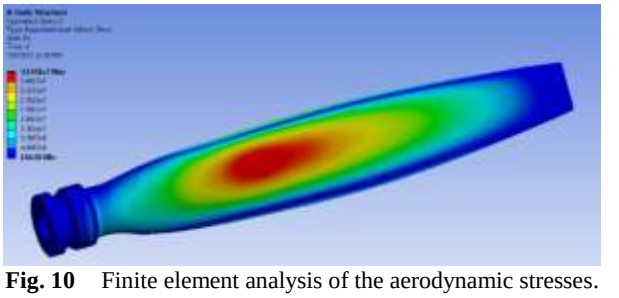

Fig. 10 Finite element analysis of the aerodynamic stresses.

To check the tension and its independence from the network and computer limitations, only the size of the blade element is reduced. Figure 11 shows changes in aerodynamic stress and "Fig. 12" shows changes in rotational dynamic stress according to element size. The variation of the stress in "Fig. 12" is negligible.

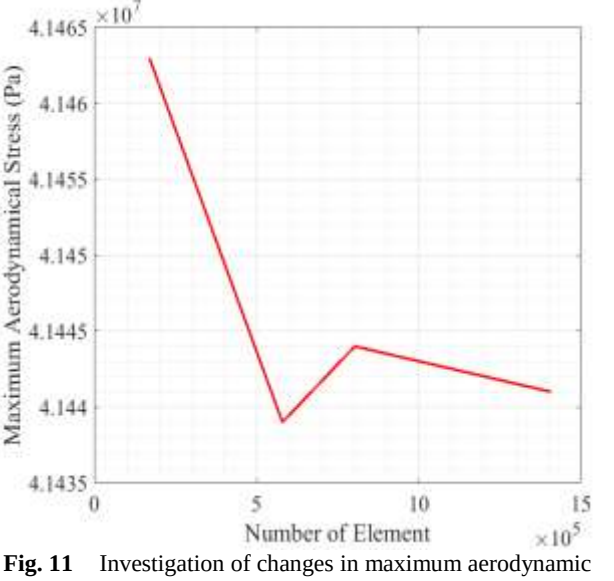

Fig. 11 Investigation of changes in maximum aerodynamic stress according to the changes in the number of blade elements.

The minimum value of stress is 158 MPa and maximum value is 168 MPa. This subject shows the convergence in the mesh dependency study.

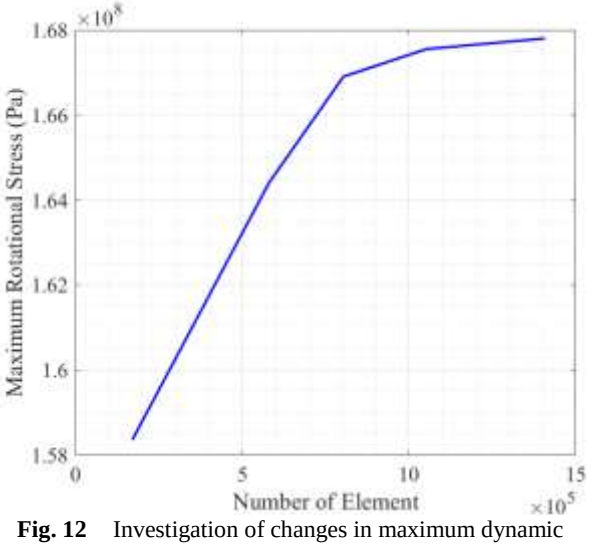

Fig. 12 Investigation of changes in maximum dynamic rotational stress according to changes in the number of blade elements.

5 DEVELOPMENTS OF A QUASI-ANALYTICAL ALGORITHM

5.1. Development of the Algorithm for Redesigning the Quasi-Propeller Geometry

Considering that the stress analysis by the quasi-analytical method requires having the closest geometry to the propeller to implement stress analysis algorithms, a quasi-propeller geometry redesign algorithm is developed. The shape of the quasi-propeller system is shown in "Fig. 13".

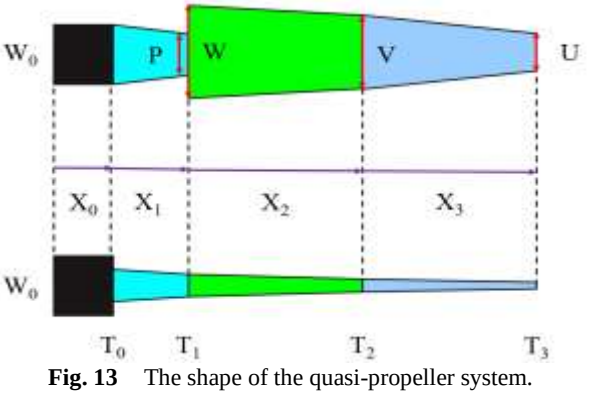

Fig. 13 The shape of the quasi-propeller system.

The performance of this method is in this way that a guess interval (such as [13.2-14.1] cm) is applied to the parameters shown in the figure with the help of 3D design software. During the algorithm, the algorithm is stopped by placing 2 numerical conditions of the total mass and the position of the center of mass. In the final selection of parameters, the most accurate mass and the most accurate center of mass will be the criteria. The range of all parameters is divided by a value of N. Therefore, the total number of design events will be equal to NM, where M is the total number of design parameters. The way the algorithm works is that it starts with the first component of the parameter X0 and with all the other components of the other parameters, the geometry is built and this work continues until the applied conditions are fulfilled. The exact mass and position of the center of mass lead to the calculation of the exact centrifugal force. The algorithm is presented in the appendix. Due to the presence of a hole in the root of the blade, in the X0 range, a certain amount of the equivalent area is reduced to fully match the reality.

5.2. Algorithms for Calculating Rotational Dynamic Forces and Stresses

5.2.1. Pure Rotational Forces and Stresses (Tensile Rotational Stress)

Due to the centrifugal force, the components of the propeller are thrown outwards. This problem causes rotational dynamic stresses in the system. The force of each element is calculated according to "Fig. 14". At any point of the blade, the dynamic equivalent stress without considering bending and in tension form is presented in "Eq. (1)".

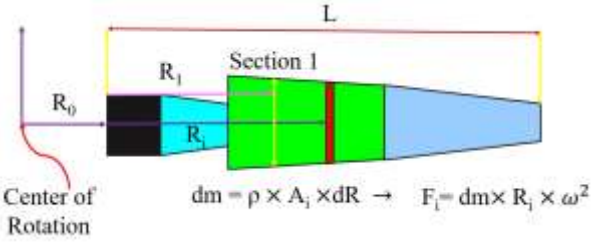

Fig. 14 Calculating the centrifugal force of each element of the blade.

$$\sigma_{Dy\,1\text{Section}1}=\frac{\int_{R_1}^{L}F_i}{A_{\text{Section}1}}=\frac{\int_{R_1}^{L}dm\times(R_i+R_0)\times\omega^2}{A_{\text{Section}1}}=\frac{\int_{R_1}^{L}\rho\times dR\times A_i\times(R_i+R_0)\times\omega^2}{A_{\text{Section}1}} \quad (1)$$

In this equation, ω is the rotational speed of the propeller, ρ is the metal density of the blade, σ is the stress, A is the cross-sectional area, L is the length of the blade, R_i is the distance of the element from the root of the propeller, and R_0 is the distance of the root from the rotation axis. The important point in the analysis is that the root of the propeller has an initial distance from the center of rotation, which is shown in "Fig. 15". In calculating the stress in the root of the propeller, the lower limit of the integral is set to 0. In the

implementation of the main algorithm, SUM is used due to the discreteness of the calculations.

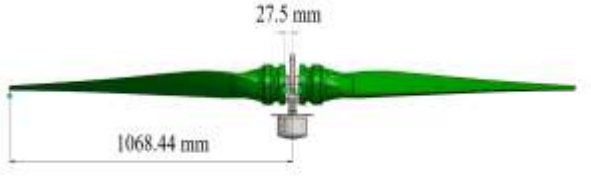

Fig. 15 The distance between the root of the propeller and the center of rotation.

5.2.2. Rotational Bending Forces and Stresses

In the previous step, the rotational dynamic net stress was calculated at each section, but each element has an eccentricity from the center line. In this case, an algorithm is developed to calculate the center of mass of each element for two non-longitudinal directions of the propeller (X is the longitudinal direction of the propeller). First, the characteristics of the center of mass in the Y and Z directions are extracted from the design software. Now, assuming the linear changes of the center of mass, two initial guesses are made for both ends of the hypothetical line, and this process is repeated in so far as the eccentricity is equal to the results of the software ("Fig. 16"). The beginning of the propeller does not have an eccentricity due to its circular nature. In addition to the circular part, the elliptical parts also do not have an eccentricity, and only the parts that are in the shape of an airfoil have an eccentricity. Since the size of the airfoils decreases from the beginning to the end of the blade, these eccentricities lead to the creation of a bending moment, because each element is thrown outward at any point. These eccentricities act like torque arms. The calculation of rotational bending stress is given in "Eq. (2)".

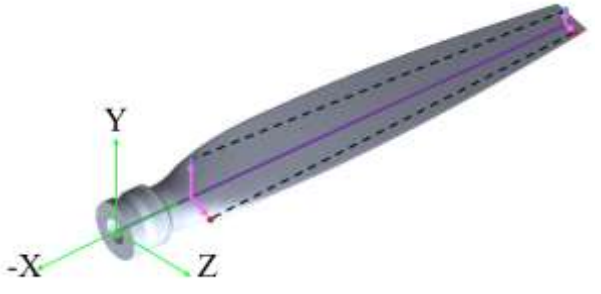

Fig. 16 Determining the eccentricity of the blade elements.

$$\sigma_{Dy\,2Section1} = \frac{Moment \times C}{I} = \frac{\int_{R_1}^{L} F_i \times E_i \times TWIST\,(i)}{\frac{I_{Section1}}{C_i}}$$
$$= \frac{\int_{R_1}^{L} dm \times (R_i + R_0) \times \omega^2 \times E_i \times TWIST\,(i)}{\frac{I_{Section1}}{C_i}} \quad (2)$$
$$= \frac{\int_{R_1}^{L} \rho \times dR \times A \times (R_i + R_0) \times \omega^2 \times E_i \times TWIST\,(i)}{\frac{I_{Section1}}{C_i}}$$

In "Eq. (2)", I is equal to the moment of inertia of each sector of the propeller, C is the distance from the neutral axes and *TWIST* is the twist angle of the propeller. In each sector, the sum of the bending stresses caused by two eccentricities is added together.

5.3. Algorithm for Calculating Aerodynamic Stresses

One of the most important structural stresses of the blade is aerodynamic stress. In this study, an algorithm is developed to calculate aerodynamic stresses. The algorithm works in such a way that it calculates the pressure difference between the two sides of each element and converts it into the equivalent force of that element and by applying the distance, it becomes its bending moment. Equation (3) shows how to calculate the aerodynamic stress in a section of the propeller. The distribution of pressure will also be in a way that creates the equivalent force of the propulsion. Also, the pressure distribution is such that the maximum pressure is created at a certain distance from the end of the propeller.

$$\sigma_{AERO\,Section1} = \frac{Moment \times C}{I}$$
$$= \frac{\int_{R_1}^{L} (P_1 - P_2) \times E_i \times TWIST(i) \times (R_i + R_0) \times dR}{\frac{I_{Section1}}{C_i}} \quad (3)$$

Equation (4) is also used to calculate the aerodynamic stresses against the rotational movement of the propeller.

$$\sigma_{AERO2Section1} = \frac{Moment \times C}{I} = \frac{\int_{R_1}^{L} (P_3 - P_4) \times E_i \times TWIST2(i) \times (R_i + R_0) \times dR}{\frac{I2_{Section1}}{C_i}} \quad (4)$$

5.4. Applying Stress Concentration Coefficients

A stress concentration coefficient should be applied to the root of the propeller, which has severe geometric changes and steps. Therefore, the algorithms are written in such a way that a stress concentration factor is applied to them. In the algorithm, a conditional order is executed that if the cross-section distance from the beginning of the propeller root is less than Z_0, the calculated bending stress values are multiplied by 2 and the tensile stress values are multiplied by 1.9. The cross-section area in the root of the propeller is minimum and also there is stress concentration. Figure 17 shows this subject.

6 RESULTS OF STRUCTURAL ANALYSIS BY QUASI-ANALYTICAL METHOD

In this part, the results of the stress analysis of the propeller are presented using the quasi-analytical method. Figure 18 shows the results. The results include the distribution of various structural parameters such as various rotational dynamic forces and moments, different aerodynamic moments, dynamic stresses, and aerodynamic stresses.

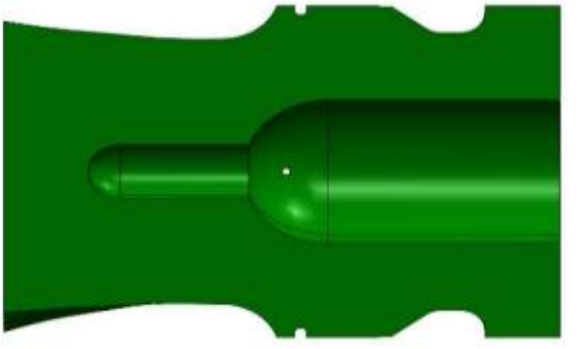

Fig. 17 Root section of the propeller and cross section area reduction.

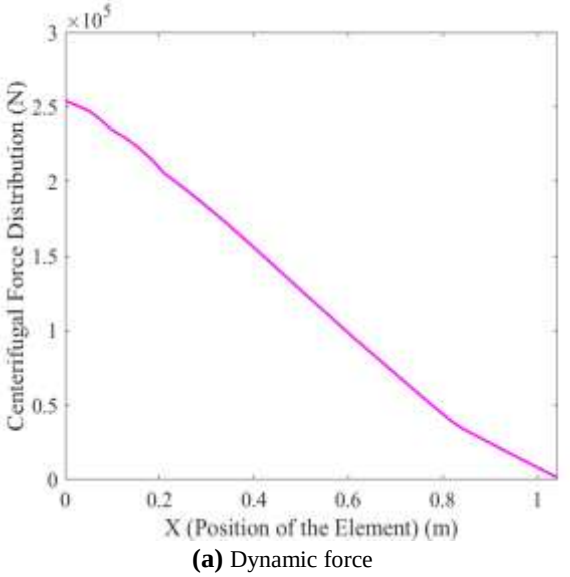

(a) Dynamic force

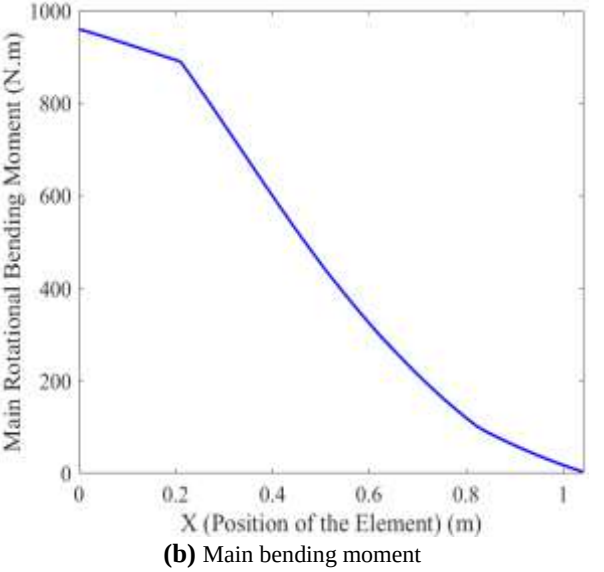

(b) Main bending moment

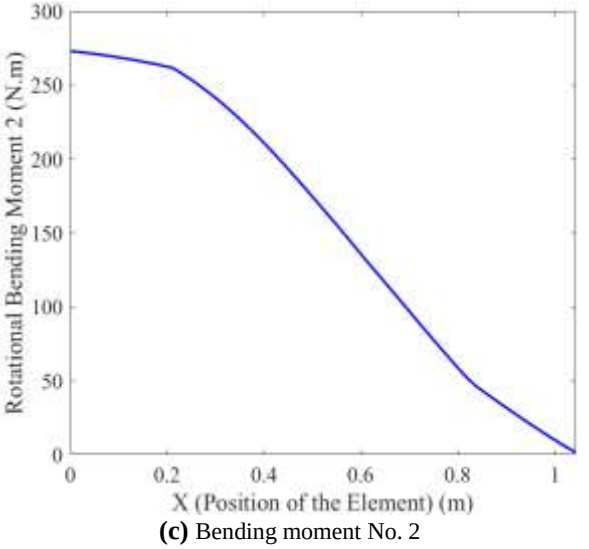

(c) Bending moment No. 2

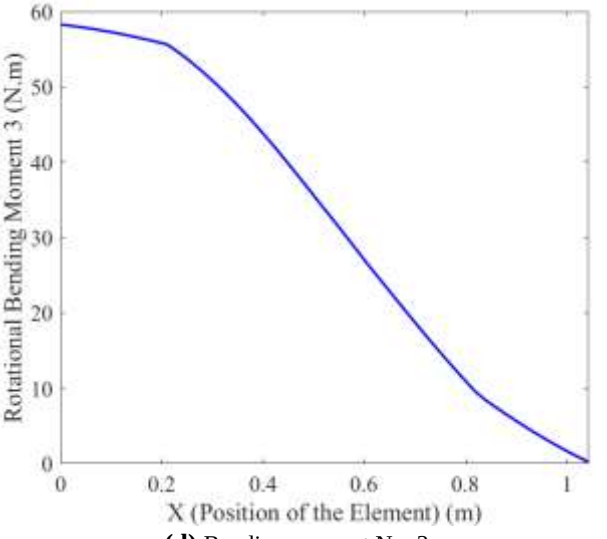

(d) Bending moment No. 3

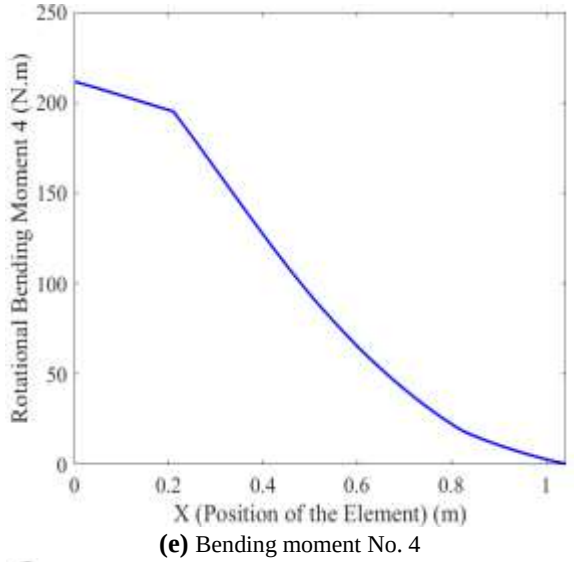

(e) Bending moment No. 4

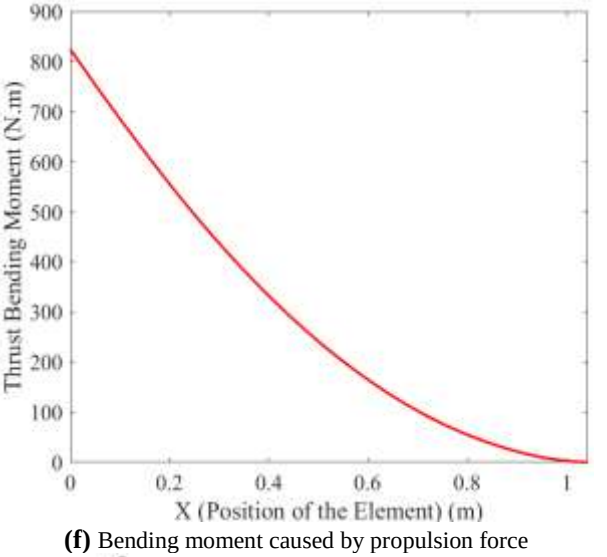

(f) Bending moment caused by propulsion force

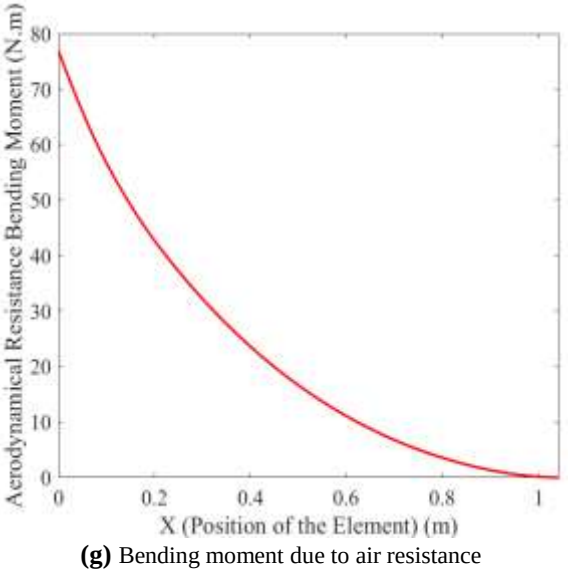

(g) Bending moment due to air resistance

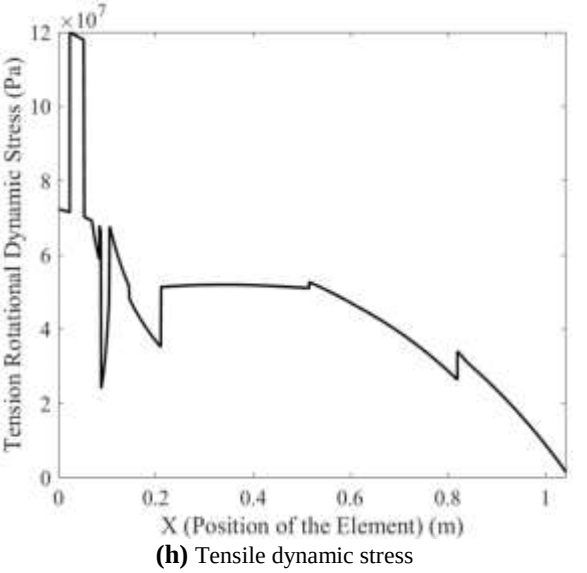

(h) Tensile dynamic stress

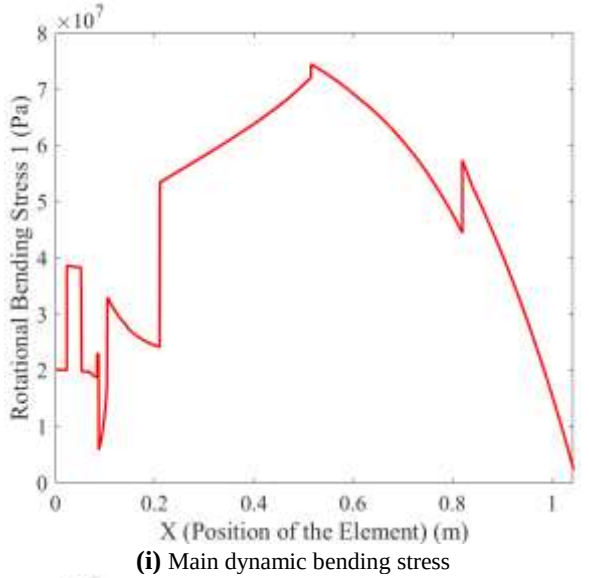

(i) Main dynamic bending stress

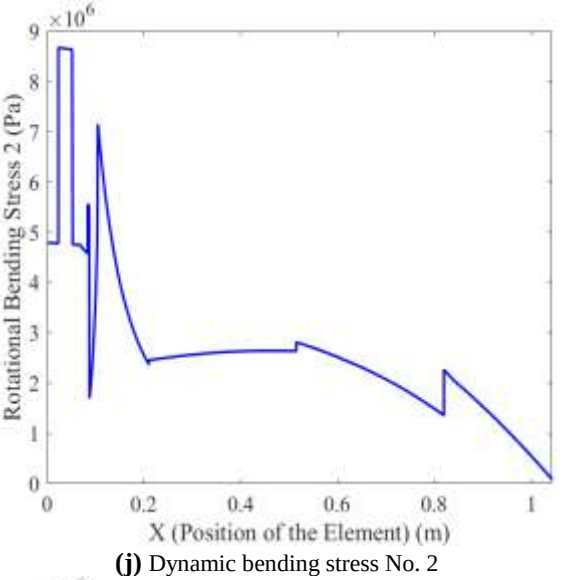

(j) Dynamic bending stress No. 2

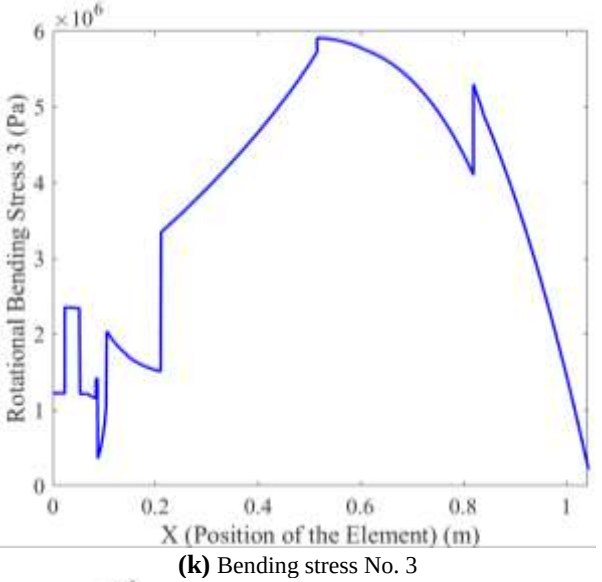

(k) Bending stress No. 3

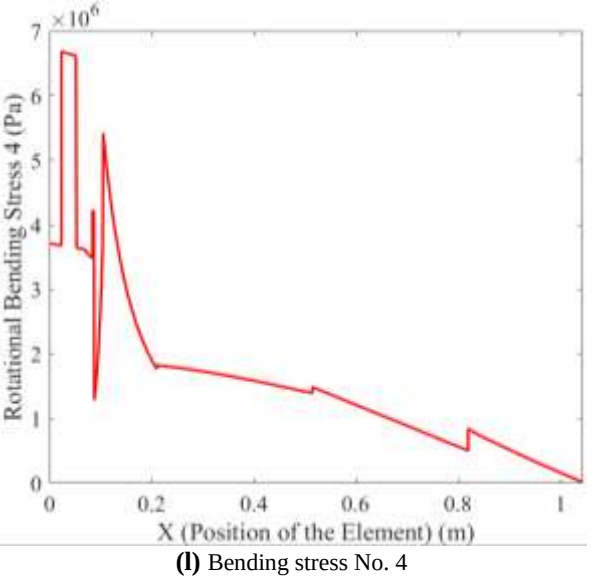

(l) Bending stress No. 4

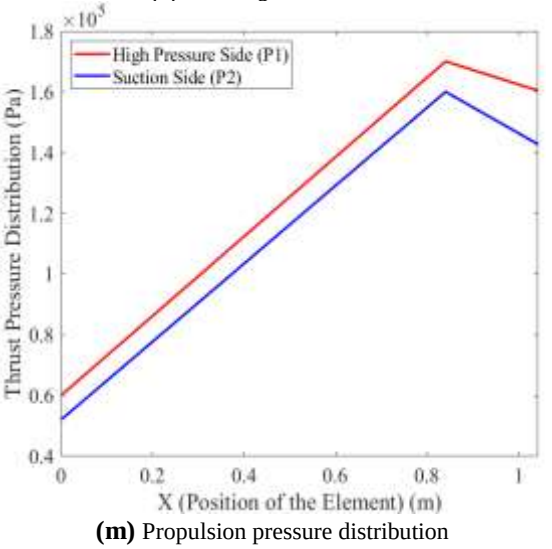

(m) Propulsion pressure distribution

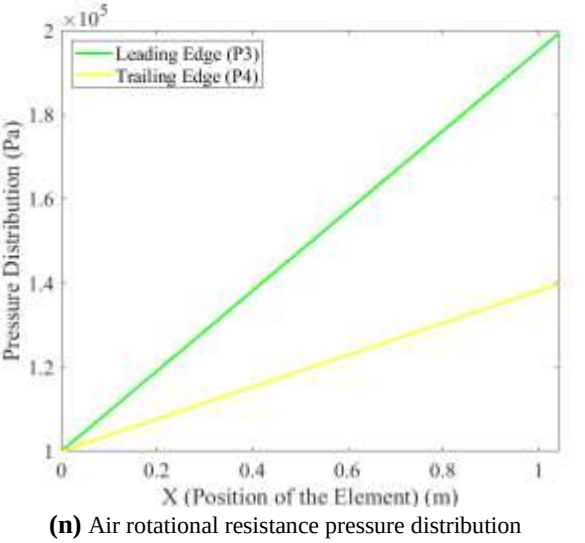

(n) Air rotational resistance pressure distribution

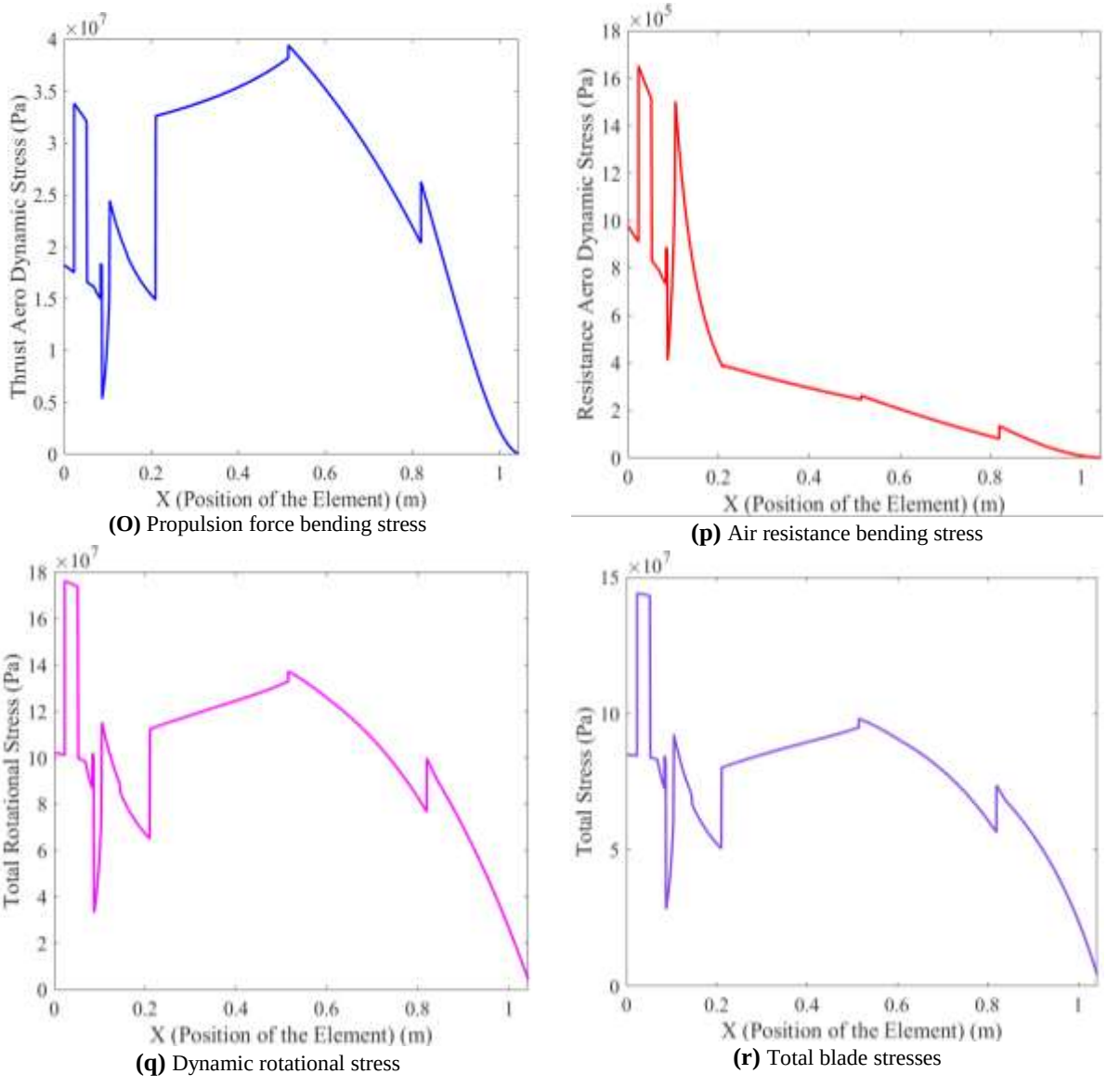

(O) Propulsion force bending stress

(p) Air resistance bending stress

(q) Dynamic rotational stress

(r) Total blade stresses

Fig. 18 Analysis of the propeller structure by quasi-analytical method and distribution of different parameters along the blade length**.**

7 EXPLAIN THE RESULTS OF THE DEVELOPED ALGORITHM

According to "Fig. 18 (a)", the maximum centrifugal force is maximum at the root of the blade. All of mass element dynamic force affects these points. Therefore, the maximum tensile force is at the root of the blade. The rotational bending moment is maximum at the root of the blade ("Fig. 18 (b, c, d, and e)") and the aerodynamical bending moment is maximum at the root of the blade ("Fig. 18 (f, g)"). According to "Fig. 18 (h)", the maximum rotational dynamic stress is the root of the blade. There is a considerable jump at the "Fig. 18 (h)". This shows that the cross-section area is significantly reduced at the root point of the blade. This subject increases the dynamic stress at this point. The maximum rotational bending stress and aerodynamic bending stress are at the center of the blade. At this point, the blade thickness is low. In bending stress, in addition to the applied bending moment, the equivalent moment of inertia is also important. In the center of the blade, the equivalent moment of inertia is much less than the root of the propeller ("Fig. 18 (i, j, k, o, p)"). The cumulative stress is presented in "Fig. 18 (q and r)". The results of the quasi-analytical method confirm the FEM method.

8 INVESTIGATING THE CAUSES OF OVERALL STRESS REDUCTION BY AERODYNAMIC LOADS

Figure 19 shows that the bending moment caused by the centrifugal force due to eccentricity and the bending moment caused by propulsion are opposite to each other. Since the rotational dynamic stresses are much more dominant, the stresses caused by the propulsion force reduce the total stresses of the system.

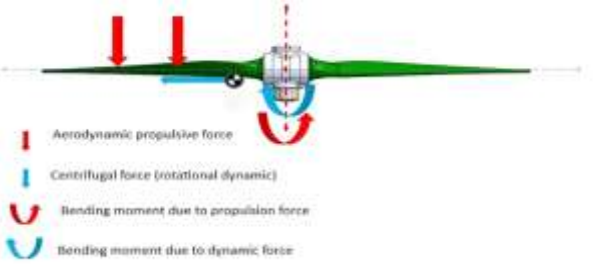

Fig. 19 Different forces and moments entering the propeller system.

9 CONCLUSIONS

In the present study, a quasi-analytical method algorithm in the geometry redesign and structural analysis of an airplane propeller was developed and compared with the finite element method. According to the results, the maximum structural stress of a propeller under rotational dynamic and aerodynamic loads is at the root of the propeller. In the case that only dynamic rotational loading is considered, the maximum stress of the propeller under dynamic loads is at the propeller root, and when only aerodynamic loading is considered, the maximum stress is at the middle of the propeller. Generally, aerodynamic stresses reduce the overall stress in the propeller because the bending moment caused by the centrifugal force due to eccentricity and the bending moment caused by the propulsion are opposite to each other. The values of rotational dynamic stress are much higher than aerodynamic stress. According to the mentioned cases, in order to increase the reliability of structural analysis, aerodynamic stresses are omitted and only rotational dynamic stresses are considered for structural analysis. Since the geometry of the propeller is constant in different working conditions and only the rotational speed changes, structural analysis can be used in the design in such a way that the maximum stress of the propeller has a direct relationship with the square power of the working rotational speed of the propeller. In this regard, if the propeller rotational speed changes to 80% of the initial speed, the structural stress will decrease to 64%. Of course, the important point is that at the maximum rotational speed, the propulsion force is maximum and at lower rotational speeds, the amount of propulsion force will also decrease. Reducing the propulsion force will reduce the aerodynamic stresses. There is a significant bending moment in the middle of the blade. The middle of blade has a weak moment of inertia relating to the root of the blade. This subject results in bending stress (aerodynamic and rotational dynamic) being maximum in the middle of the blade.

APPENDIX: PRESENTATION OF THE STRUCTURAL ANALYSIS ALGORITHMS USING A QUASI-ANALYTICAL METHOD

In order to define blade geometry to structural analysis algorithm, the total geometry redesigned by the quasi-blade redesigning algorithm is presented in "Fig. 20".

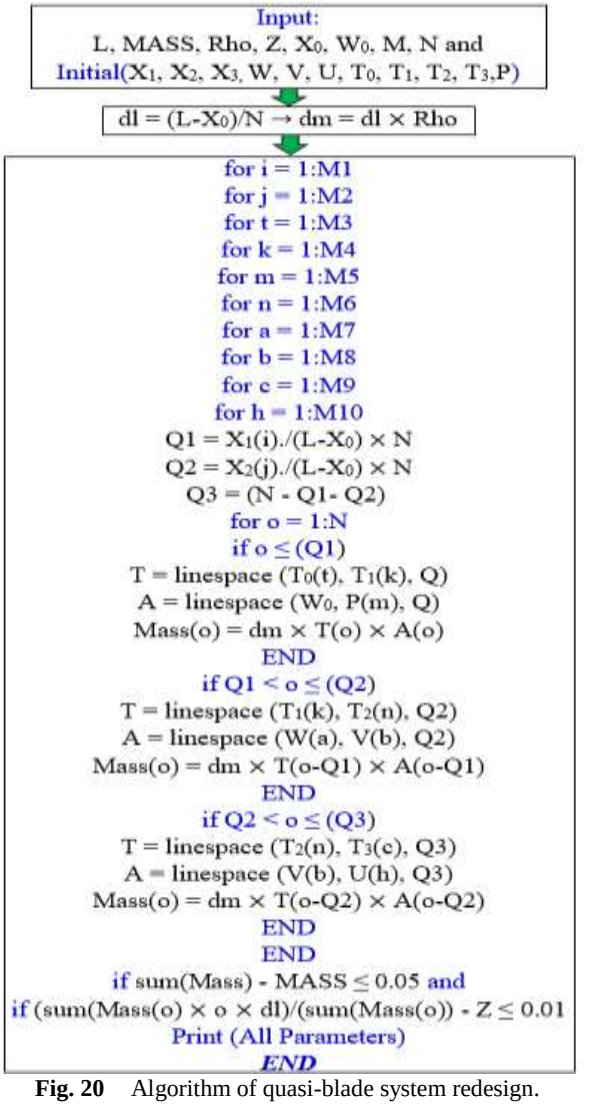

Fig. 20 Algorithm of quasi-blade system redesign.

The main dimension in "Fig. 13" is changed by the

algorithmic try and error process. In this regard, the dimensions such as X, W, and T has own intervals. The size of each dimension is M, which M is matrix → M = [M1:M10]. The X2 and X3 are dependent on the X and L. The thickness matrix (T) and Area of cross-section (A), the Q1 and Q2 are calculated. T and A matrix construct the Mass matrix. The algorithm continues till the total mass was acceptable.

In order to calculate the cross-section area, mass, and moment of inertia distribution, mass and area-inertia algorithm is developed and presented in "Fig. 21". The root of blade with length of X0 affects the total mass. The Line1 = [X0, X1, X2, X3] and Line2 = [T0, T1, T2, T3]. The root of the blade has a circular cross-section and the other part of the blade has a rectangular (airfoil) cross-section. Therefore, the algorithm consists of two parts, before and after M.

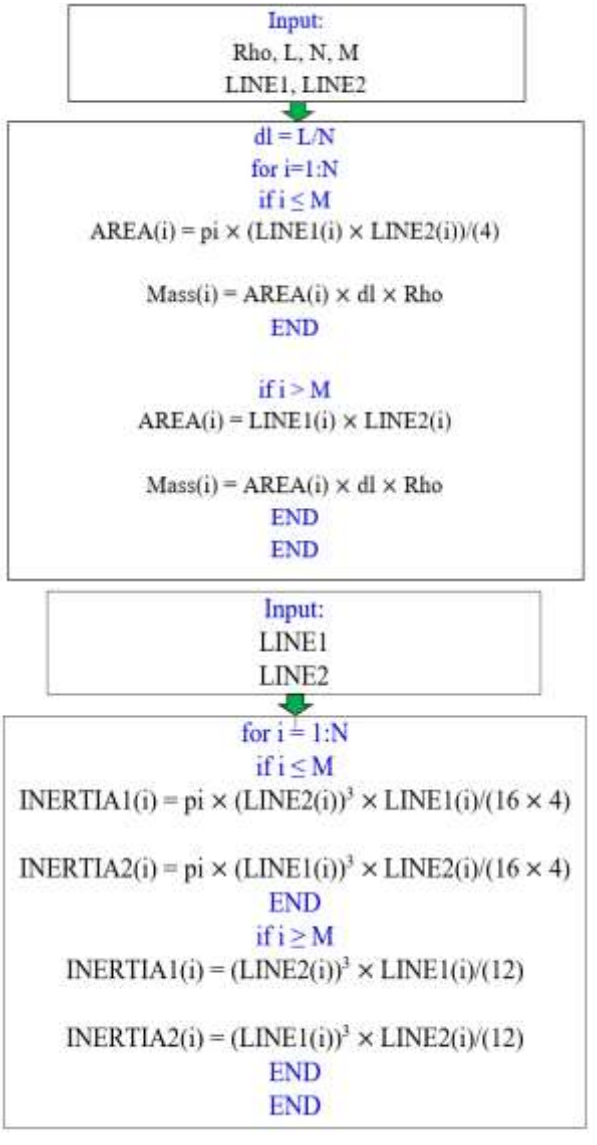

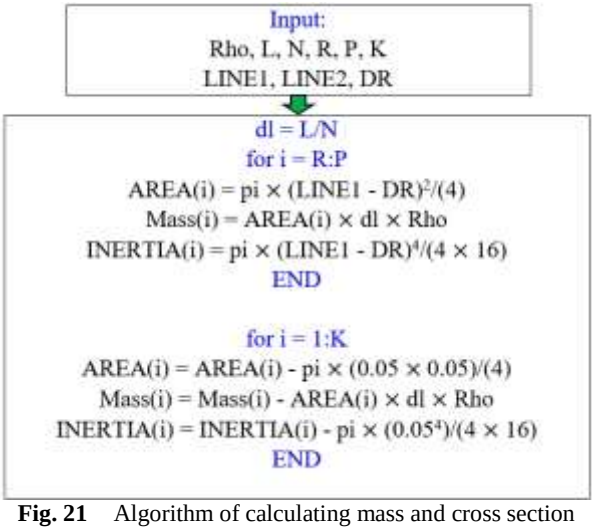

Fig. 21 Algorithm of calculating mass and cross section area and moment inertia.

The algorithm of calculating the dynamic force and tensile dynamic stress distribution is presented in "Fig. 22".

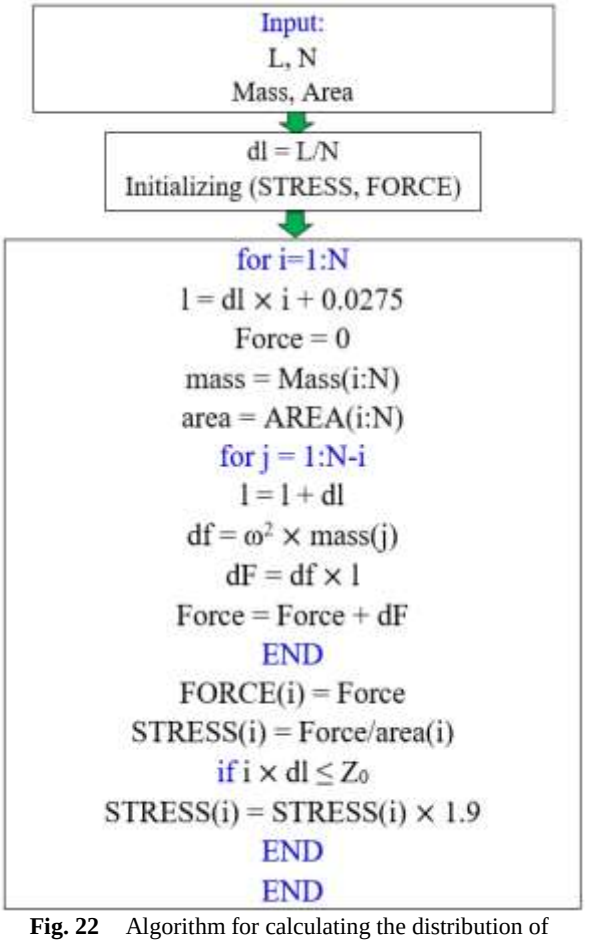

Fig. 22 Algorithm for calculating the distribution of dynamic force and tensile dynamic stress along the blade length.

There is one loop for all sections in the blade and there is an internal loop for each section. In each section, all of the element which affects stress must be considered. This subject was used in "Fig. 14" and Equation (1). This algorithm converts the continuous integral to discrete SUM. The distance of each element and center of rotation is calculated by the sum of previous elements lengths and also 0.0275. This subject was showed in "Fig. 15". According to stress concentration at the root of the blade, the algorithm has this section at the end of calculation.

The centrifiugal force also results in the bending moment and bending stress in the each section of the blade. Figure 23 presents the calculation of the bending stress of the blade. This algorithm is based on the previous algorithm ("Fig. 22"). In this algorithm, the dynamic force of each element results in the bending and is a function of dynamic force (df1) and arm of the moment (Eccen). Considering the twisting of the blade, the final moment multiplies the sin(Twist). The excentricity of blade sections is shown in "Fig. 16". According to the stress concentration at the root of the blade, the algorithm has this section at the end of the calculation.

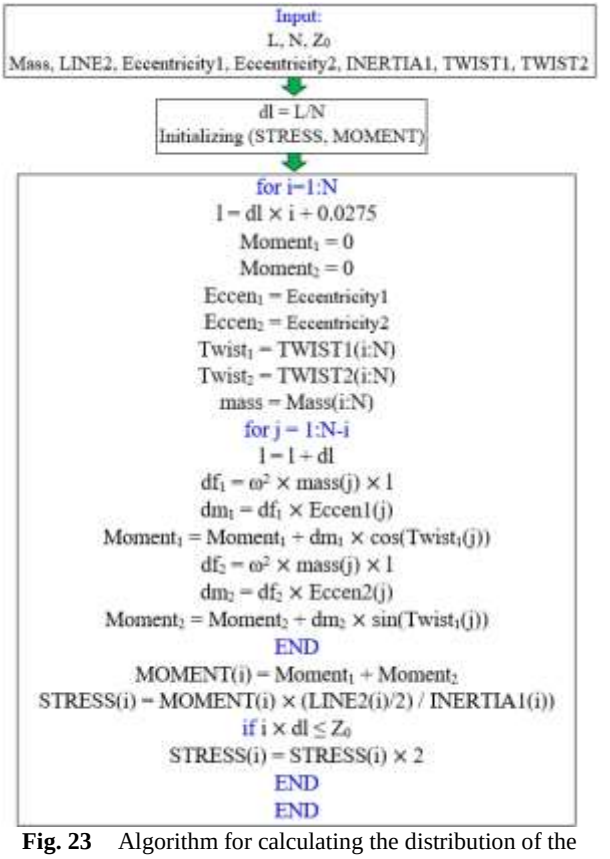

Fig. 23 Algorithm for calculating the distribution of the dynamic bending moment due to eccentricity in a certain direction from the propeller and the dynamic bending stress along the blade length.

Figure 24 presents the calculation of aerodynamics stress. This algorithm is similar to the previous algorithm. The difference between these algorithms is the bending moment. The bending moment of aerodynamics load is based on differential pressure. The differential pressure on each element leads to aerodynamic force. This dynamic force on each element results bending moment along the blade. The Twisting and stress concentration also are considered in this part. The P3 is related to leading-edge pressure, and P4 is related to the trailing edge. The P1 and P2 are differential pressures relating to high and suction pressure zones.

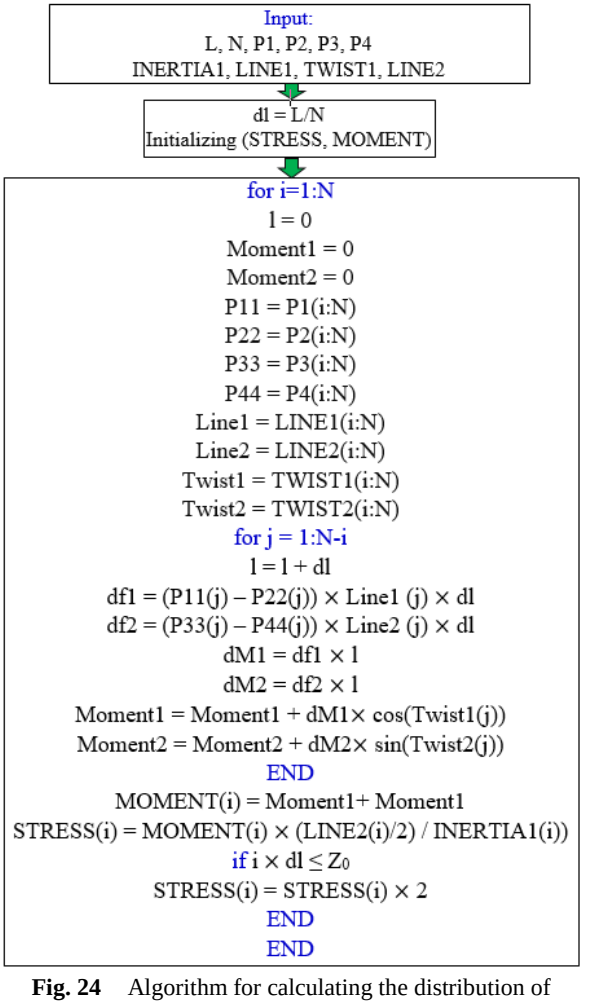

Fig. 24 Algorithm for calculating the distribution of bending moment due to aerodynamic pressure to produce propulsive force and rotational resistance of air and the resulting bending stresses.

REFERENCES

[1] Yeh, M. K., Wang, C. H., Stress Analysis of Composite Wind Turbine Blade by Finite Element Method, IOP Conference Series: Materials Science and Engineering, Vol. 241, 2017, pp. 12-15.

[2] Srivastava, S., Roy, A. K., and Kumar, K., Design of a Mixed Flow Pump Impeller Blade and Its Validation Using Stress Analysis, Procedia Materials Science, Vol. 6, 2014, pp. 417-424.

[3] Wu, W. H., Young, W. B., Structural Analysis and Design of The Composite Wind Turbine Blade, Applied Composite Materials, Vol. 19, 2012, pp. 247-257.

[4] Duan, W., Zhao, F., Loading Analysis and Strength Calculation of Wind Turbine Blade Based on Blade Element Momentum Theory and Finite Element Method, Asia-Pacific Power and Energy Engineering Conference, IEEE, 2010, pp. 1-4.

[5] Yeh, M. K., Cheng, Y. C., and Wang, C. H., Finite Element Stress Analysis of Wind Blade Structure Under Wind Pressure, Taiwan Wind Energy Conference, Taipei, Taiwan, No. SI_07, 2015 (in Chinese).

[6] Heo, H., Ju, J., and Kim, D. M., Compliant Cellular Structures: Application to A Passive Morphing Airfoil, Composite Structures, Vol. 106, 2013, pp. 560-569.

[7] Di, T., Zhiliang, L., and Tongqing, G., Aeroelastic Analysis of Large Horizontal Wind Turbine Blades, Applied Mathematics and Mechanics (English Edition), Vol. 37(S1), 2016, pp. S97-S104.

[8] Metallic Material Properties Development and Standardization (MMPDS) Handbook, Battelle Memorial Institute, 2019.

[9] Behzad, M., Izanlo, H., Arghand, H., Davoodabadi, A., and Saleh, A., Bearing Housing Looseness Effect on Rotating Machinery Vibration, 29th International Congress on Sound and Vibration, 2023.